THE ASTROPHYSICAL JOURNAL, 493:L67–L70, 1998 February 1

SPECTRAL PROPERTIES OF THE PROMPT X-RAY EMISSION AND AFTERGLOW FROM THE GAMMA-RAY BURST OF 1997 FEBRUARY 28

F. FRONTERA,[1,2] E. COSTA,[3] L. PIRO,[3] J. M. MULLER,[4,5] L. AMATI,[3] M. FEROCI,[3] F. FIORE,[5] G. PIZZICHINI,[1] M. TAVANI,[6,7] A. CASTRO-TIRADO,[8] G. CUSUMANO,[9] D. DAL FIUME,[1] J. HEISE,[4] K. HURLEY,[10] L. NICASTRO,[1] M. ORLANDINI,[1] A. OWENS,[11] E. PALAZZI,[1] A. N. PARMAR,[11] J. IN'T ZAND,[4] AND G. ZAVATTINI[2]

Received 1997 August 29; accepted 1997 November 21; published 1998 January 14

ABSTRACT

We report high-energy spectral data of the prompt emission of GRB 970228 and its X-ray afterglow. We establish that the nature of the X-ray afterglow emission is nonthermal and similar to the later portion of GRB 970228. Our data can be used to discriminate different emission models of GRB afterglows. While cooling of excited compact objects can be ruled out, fireball models are constrained in the physics of the radiation emission processes and their evolution.

Subject headings: gamma rays: bursts — gamma rays: observations — stars: neutron — X-rays: general

1. INTRODUCTION

Recent observations of the GRB 970228 afterglow (Costa et al. 1997a) by the *BeppoSAX* satellite (Boella et al. 1997) have shown that it may be actually possible to identify the ultimate source and nature of emission of gamma-ray bursts (GRBs). Eight hours after the burst, we detected a new transient X-ray source, 1SAX J0501.7+1146, by repointing the *BeppoSAX* narrow field instruments (NFIs) at the GRB location. Various arguments render compelling the interpretation of this source in terms of a fading X-ray afterglow from GRB 970228: (1) the backward extrapolation of the source light curve to the time of the burst is consistent with the average X-ray flux detected during the late phase of the burst (Costa et al. 1997b); (2) its celestial position is consistent with the burst position determined by the Interplanetary Network (Hurley et al. 1997); (3) a fading optical transient consistent with both the Wide Field Camera's (WFC) and NFIs' positions was also discovered (van Paradijs et al. 1997; Guarnieri et al. 1997); (4) an observation of the GRB error box with *ROSAT* provided the position of the X-ray transient source within a 10″ radius. Its centroid coincides, within 2″, with the optical transient position (Frontera et al. 1997b, 1997c). The optical transient appears to be embedded in an apparently constant extended source (Sahu et al. 1997). If it is a galaxy, those models that place GRBs at cosmological distances would be favored.

In another paper (Costa et al. 1997b), we reported the decay of the light curve of the source, which is described by a power-law function ($\propto t^{-\alpha}$ with index $\alpha = 1.33^{+0.13}_{-0.11}$) that is consistent with that expected in simple relativistically expanding fireball models (Wijers, Rees, & Mészáros 1997). In this Letter we report on the spectral evolution of GRB 970228 and its afterglow.

2. OBSERVATIONS

GRB 970228 was detected by the Gamma-Ray Burst Monitor (GRBM, 40–700 keV) (Frontera et al. 1997a) and WFC no. 1 (1.5–26.1 keV) (Jager et al. 1997) on board *BeppoSAX* on February 28.123620 UT (Costa et al. 1997a). Its position was determined to be within an error radius of 3′ (3 σ) centered at $\alpha_{2000} = 05^{h}01^{m}57^{s}$, $\delta_{2000} = 11^{\circ}46'24''$. Eight hours after the initial detection, the NFIs on board *BeppoSAX* were pointed at the burst location for a first target of opportunity (TOO1) observation from February 28.4681 to 28.8330 UT. A new X-ray source, 1SAX J0501.7+1146, was detected (Costa et al. 1997b) in the GRB error box by both the low-energy (0.1–10 keV, 8725 s exposure time) and medium-energy (2–10 keV, 13444 s) concentrator spectrometers (LECS and MECS, respectively). The same field was again observed about 3 days later for a second observation (TOO2) from March 3.7345 to 4.1174 (16270 s MECS and 9510 s LECS). During this observation, the 2–10 keV source flux had decreased by about a factor of 20. The main arguments for the association of this source with the X-ray afterglow of GRB 970228 have been discussed in § 1.

The data available from GRBM for spectral analysis include two 1 s ratemeters (40–700 and >100 keV) and 128 s count spectra (40–700 keV, 225 channels). The energy resolution of the GRBM unit 1, co-aligned with WFC no. 1, is 20% at 280 keV (Amati et al. 1997). WFCs (energy resolution ≈20% at 6 keV) were operated in normal mode with 31 channels in 1.5–26 keV and 0.5 ms time resolution (Jager et al. 1997). The burst direction was offset by 14° with respect to the WFC axis. The effective area of the GRBM unit 1, co-aligned with WFC no. 1, is ≈420 cm^2 in the 40–700 keV band and is ≈500 cm^2 at 300 keV. The corresponding effective area of WFC no. 1 averaged in the 2–26 keV energy band is 118 cm^2. The background level in the WFC and GRBM energy bands was variable during the burst (Feroci et al. 1997). This variation was apparent up to 100 keV, while above 100 keV the background

[1] Istituto Tecnologie e Studio Radiazioni Extraterrestri, CNR, Via Gobetti 101, 40129 Bologna, Italy.
[2] Dipartimento di Fisica, Università di Ferrara, Via Paradiso 12, 44100 Ferrara, Italy.
[3] Istituto Astrofisica Spaziale, CNR, Via E. Fermi 21, 00044 Frascati, Italy.
[4] Space Research Organization in the Netherlands, Sorbonnelaan 2, 3584 CA Utrecht, The Netherlands.
[5] *BeppoSAX* Scientific Data Center, Via Corcolle 19, 00131 Roma, Italy.
[6] Istituto Fisica Cosmica e Tecnologie Relative, CNR, Via Bassini 15, 20133 Milano, Italy.
[7] Columbia Astrophysics Laboratory, Columbia University, New York, NY 10027.
[8] Laboratorio de Astrofìsica Espacial y Fìsica Fundamental, P. O. Box 50727, 28080 Madrid, Spain.
[9] Istituto Fisica Cosmica e Applicazioni all'Informatica, C.N.R., Via U. La Malfa 153, 90146 Palermo, Italy.
[10] University of California, Berkeley, Space Science Laboratory, Berkeley, CA 94720-7450.
[11] Astrophysics Division, Space Science Department of ESA, ESTEC, Noordwijk, The Netherlands.

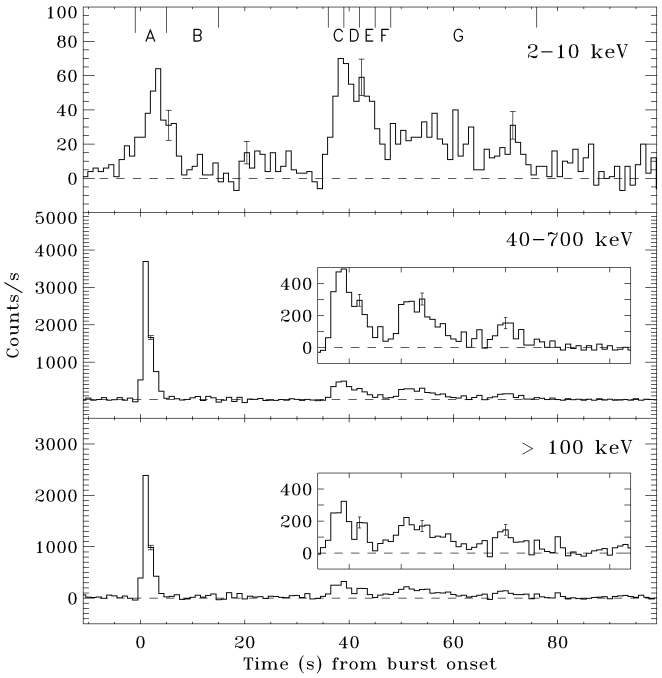

FIG. 1.—Light curve of GRB 970228 in different energy bands, after background subtraction (see text). Dashed lines give the background reference. In the insets, the three minor pulses of the burst are shown. The time sections on which the spectral analysis was performed are shown on the top.

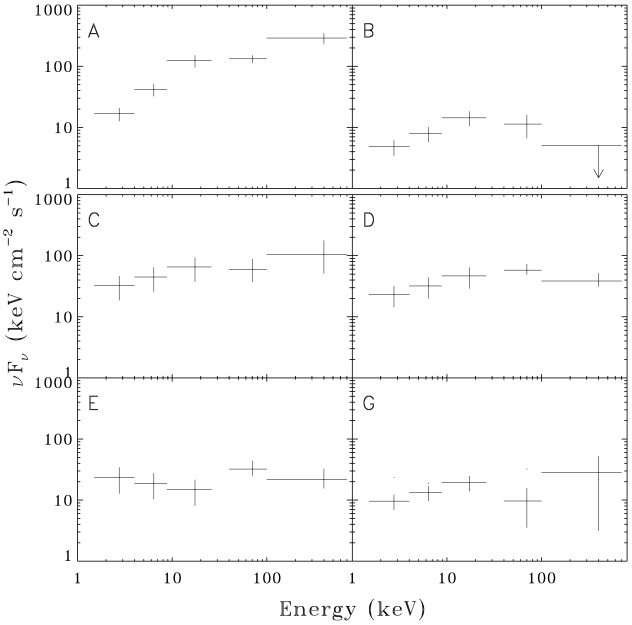

FIG. 2.—νF_ν spectrum of the burst (ν is the photon energy in keV and F_ν is the specific energy flux in keV cm^{-2} s^{-1} keV^{-1}) for six of the seven time sections in which we divided the burst time profile. The time intervals from the burst onset over which the spectrum has been accumulated are also shown.

was stable. For the WFC spectra and light curves, the background level was estimated using an equivalent section of the detector area not illuminated by the burst. In the case of GRBM, background during the burst was estimated by interpolation, using a quadratic function that fitted the 150 s count rate data before the burst and the 100 s data after its end. The presence of a variable background prevented the derivation of useful upper limits to the afterglow emission after the burst. During TOO1, the X-ray source associated with the burst afterglow was offset by about 10′ with respect to the telescope axes. Since the image centroid, for MECS 1 and 2, coincided with a strong-back that supports the detector window and absorbs most photons up to about 6 keV, we used for the spectral analysis only MECS 3 and LECS. The LECS and MECS spectra for TOO1 were extracted from a 4′ radius region around the centroid of the image source. For TOO2, the source was on-axis, and the spectra from LECS and MECS were extracted from a 2′ radius region. The MECS spectra were equalized and added together. The background spectrum was estimated from long observations (200 ks for MECS and 100 ks for LECS) of blank sky fields, using an equivalent detector region of the source image with a similar offset.

Figure 1 shows the time profiles of GRB 970228 in different energy bands after the background subtraction. In the γ-ray energy band (40–700 keV), the burst is characterized by an initial 5 s strong pulse followed, after 30 s, by a set of three additional pulses of decreasing intensity. In the X-ray band (1.5–10 keV) the first pulse starts within 1 s of the γ-ray pulse, achieves the peak flux later, and has a duration 3 times longer. The entire burst duration is ~80 s. The γ-ray (40–700 keV) fluence of the entire burst is $(1.1 \pm 0.1) \times 10^{-5}$ ergs cm^{-2}, which is a factor of 5 ± 1 higher than the corresponding value in the 2–10 keV band. (This ratio is based on the more accurate analysis of the WFC data performed for this Letter and corrects the approximate value given previously by Costa et al. 1997b). For comparison, the 40–700 keV fluence integrated over the first pulse is $(6.1 \pm 0.2) \times 10^{-6}$ ergs cm^{-2}, which is a factor of 8.5 ± 1.3 higher than the corresponding fluence in 2–10 keV. The γ-ray peak flux is $(3.7 \pm 0.1) \times 10^{-6}$ ergs cm^{-2} s^{-1}, while the corresponding 2–10 keV flux is $(1.4 \pm 0.1) \times 10^{-7}$ ergs cm^{-2} s^{-1}, with a ratio between γ-ray and X-ray peak fluxes of 26 ± 2. In the BATSE energy band (50–300 keV) the fluence of GRB 970228 is 6.1×10^{-6} ergs cm^{-2}.

3. SPECTRAL ANALYSIS AND RESULTS

We divided the GRB time profile into seven temporal sections and performed a separate spectral analysis on the average spectrum of each section. The duration of the sections were chosen on the basis of the statistical quality of the data. In particular, we obtained two spectra (5 and 9 s duration, respectively) for the first pulse (A and B in Fig. 1), four 3 s spectra for the second pulse (C, D, E, and F), and only one spectrum for the third and fourth pulses together (G in Fig. 1). All WFC spectra are well fitted with power laws ($K_X E^{\alpha_X}$), while blackbody spectra do not fit the data. We assumed power laws ($K_\Gamma E^{\alpha_\Gamma}$) to deconvolve spectral data in the GRBM band. In Figure 2 we show the logarithmic power per photon energy decade (the νF_ν spectrum) for six of the time intervals defined above. The spectral evolution of the first GRB pulse and its diversity from the subsequent pulses are evident. The initial part of the first pulse (Fig. 2*a*) is quite hard, with noticeable curvature of the νF_ν spectrum. The peak energy, which is not detectable in the WFC/GRBM energy range, is likely above 700 keV. The decay part of the first pulse (Fig. 2*b*) shows substantial evolution, with a clearly detectable broad curvature. By fitting the photon spectrum with a smoothly broken power law (Band et al. 1993), we found a peak energy at $E_p = 35 \pm 18$ keV. This peak energy behavior is typical of GRB spectral evolution (Ford et al. 1995). In Figure 3 we show the time evolution from the burst onset of the GRBM and WFC

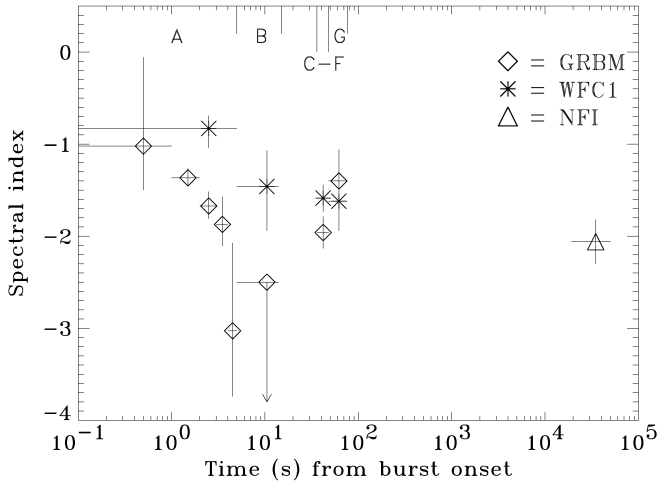

FIG. 3.—Behavior of the X-ray and γ-ray power-law photon indices with time from the burst onset. The photon index of the X-ray afterglow spectrum is also shown.

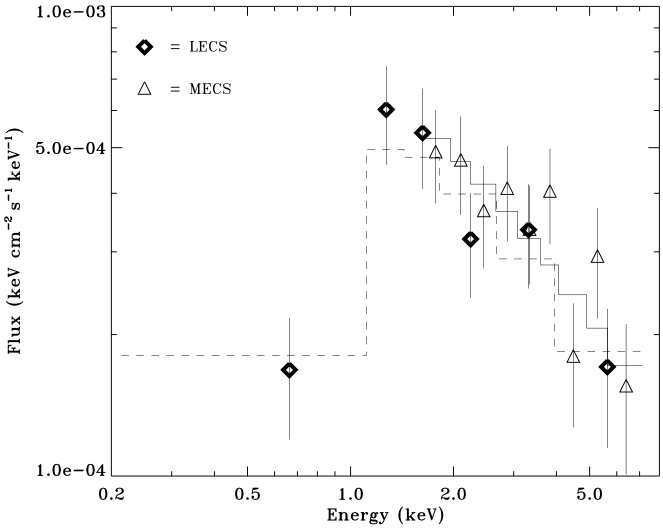

FIG. 4.—Deconvolved LECS and MECS spectra of the X-ray afterglow during TOO1. The best-fitting power-law model with low-energy photoelectric absorption is superposed to the LECS (*dashed line*) and MECS (*full line*) data.

power-law spectral indices α_Γ and α_X. For the first pulse, the temporal behavior of α_Γ is well described by a linear law [$\alpha_\Gamma(t) = a + bt$, $\chi^2 = 1.28$, 3 dof] with $a = -0.9 \pm 0.2$ and $b = -0.31 \pm 0.05$, and t in seconds. The power-law photon indices α_Γ and α_X do not evolve in the same way as a consequence of the curvature of the first pulse spectra. We also note the interesting spectral softening during the decaying part of the pulse.

The spectral behavior of the second pulse is significantly different from that of the first one. The spectral data can be fitted with a single power law over the 1.5–700 keV range. During the first 3 s of the second pulse, the spectrum (Fig. 2*c*) is significantly harder than during the last part of the first pulse. The photon index α_Γ of the second pulse versus time from pulse onset shows some evidence of evolution (it can be fitted with a linear law as above with $a = -1.6 \pm 0.2$ and $b = -0.12 \pm 0.04$), but it is also consistent with a constant value. Instead α_X is definitely constant during the second pulse. The overall WFC/GRBM photon index of the second pulse is initially -1.8 ± 0.1 and then -1.9 ± 0.1. Interestingly, there is no strong evidence for spectral curvature as shown in Figures 2*c*, 2*d*, and 2*e*, probably indicating that the peak energy E_p passed through the WFC/GRBM energy band during the first part of the burst and, as a consequence, later it is below ~2 keV. Low counting statistics prevents us from deriving good quality spectra for the last section of the second pulse (section F) and for the third and fourth pulses, separately. For section F (not shown in Fig. 2), the X-ray data were fitted by a power-law model with $\alpha_X = -1.5 \pm 0.4$, while the γ-ray data provided only a 2 σ upper limit of the α_Γ spectral index of -0.6. The average photon spectrum of the sum of the third and fourth is well fitted with a power-law model of $\alpha_\Gamma = -1.4^{+0.5}_{-0.3}$ and $\alpha_X = -1.6 \pm 0.1$. It appears that the spectrum is again harder than that at the end of the second pulse and more similar to the one at the beginning of the second pulse. In any case, it is consistent with a single power law. The νF_ν spectrum of the sum of the third and fourth pulses is shown in Figure 2*g*.

Remarkably, we find that the power-law spectral model continues to hold also during the X-ray afterglow. The photon spectrum of 1SAX J0501.7+1146 in the 0.1–10 keV energy band as measured during the TOO1 observation is shown in Figure 4. It was obtained from the source count spectra of LECS and MECS after deconvolution for the instrument responses. Spectral fits were performed with the XSPEC 9.0 package. We fitted various functions to the source count rate spectrum (see Table 1). The best-fitting model, with a $\chi^2 = 7.2$ (10 dof) is a power law of photon index $\alpha = 2.06 \pm 0.24$ and photoelectric absorption $N_H = 3.5^{+3.3}_{-2.3} \times 10^{21}$ cm^{-2}. A power-law model with $N_H = 0$ does not fit the data, nor does an absorbed blackbody model. The probability that the difference in the χ^2 between these models and the absorbed power law is due to chance is 1.2×10^{-3} and 7.2×10^{-4}, for the power law with $N_H = 0$ and for the absorbed blackbody, respectively. Our determination of N_H is consistent with the total Galactic photoelectric absorption (~1.6×10^{21} cm^{-2}) expected along the line of sight to the GRB error box. We can exclude a nearby source with zero equivalent N_H (e.g., near the solar system) at about 3 σ statistical significance. In Figure 4, we also show the best-fitting model spectrum of the X-ray afterglow. During the TOO2 observation, the X-ray source was too

TABLE 1

SPECTRAL FITS OF 1SAX J0501.7+1146 IN THE ENERGY RANGE 0.1–10 keV[a]

Model	A[b]	α	kT (keV)	N_H ($\times 10^{21}$ cm^{-2})	χ^2	dof
Power law plus abs[c]	$1.19^{+0.87}_{-0.50}$	2.06 ± 0.24	...	$3.5^{+3.3}_{-2.3}$	7.2	10
PL with abs set to 0	0.52 ± 0.15	0.45 ± 0.20	...	0 (frozen)	17.8	11
Blackbody plus abs[c]	0.032 ± 0.005	...	0.86 ± 0.12	0^{+1}	18.7	10

[a] Uncertainties at the 90% confidence level for a single parameter.
[b] Photons cm^{-2} s^{-1} keV^{-1} at 1 keV.
[c] Photoelectric absorption of a gas with cosmic abundance (Morrison & McCammon 1983).

weak to derive a high-quality spectrum. The MECS detected a 2–10 keV flux of $(1.5 \pm 0.5) \times 10^{-12}$ ergs cm^{-2} s^{-1} from the source, while the LECS did not detect any significant flux (3 σ upper limit of 0.4×10^{-12} ergs cm^{-2} s^{-1}). The hardness ratio HR_1 between the count rate in the hard X-ray band (2–10 keV) and that in the soft band (0.1–2 keV) is 2.5 ± 0.8 for TOO1 and in excess of 2.5 for TOO2 (3 σ lower limit). However, the hardness ratio HR_2 between two hard X-ray bands (3–5 keV and 1.5–3 keV) does not show statistically significant variations from the first to the second TOO observation. Thus, we cannot infer a change in the spectral shape from TOO1 to TOO2.

4. DISCUSSION AND CONCLUSIONS

The nonthermal spectrum of the burst radiation and of the X-ray afterglow is the most important result of this analysis. A power-law model was found to fit the spectral data better than a blackbody model. The maximum value of α_Γ (-0.9 ± 0.2) achieved at the onset of the first pulse as well as the corresponding α_X during the first 5 s are consistent with the asymptotic spectral index below the peak energy E_p (-0.67), as expected in synchrotron emission models (e.g., the synchrotron shock model, or SSM; Tavani 1996). The spectral index of the first pulse rapidly evolves to $\alpha_\Gamma = -2.3 \pm 0.3$ at the end of the γ-ray pulse. In the SSM framework the final value of α_Γ during the first pulse corresponds to an index of the nonthermal electron energy distribution function $\delta = 3.7$. During the first 3 s of the second pulse the spectrum is significantly harder than during the last part of the first pulse. This indicates significant reenergization or relaxation of the particle energy distribution function within the ~20 s between the first and the second pulse. It appears that the last three GRB pulses and the X-ray afterglow have a similar nonthermal spectrum and that this spectrum does not appear to change from the first to the second TOO. These results are not consistent with simple cooling models of excited compact objects. An analysis of *Ginga* data suggested the existence of blackbody spectral components in the "precursor" or "delayed" GRB emission in the 1–10 keV band (Yoshida et al. 1989; Murakami et al. 1991). In this burst we find no evidence for a blackbody spectral component of temperature ~1–2 keV or for a prominent soft X-ray component. Furthermore, there is no evidence of upturn in the soft X-ray intensity with respect to the higher energy spectrum (Liang et al. 1997).

An evolving nonthermal spectrum for both the burst and afterglow emission is generally expected in relativistic expanding fireball models (Mészáros & Rees 1997; Tavani 1997). In these models, the physics and locations of the shocks associated with the fireballs heavily influence the photon emission mechanisms. Simple fireball models, in which only the forward blast wave radiates efficiently, predict an evolution of the peak energy as a function of the time t from the burst onset, $E_p \propto t^{-3/2}$ (Tavani 1997; Wijers et al. 1997). By extrapolating our data for the first pulse of GRB 970228, we obtain an initial $E_p \simeq 1$ MeV. In this model, the overall evolution of the X-ray intensity is expected to evolve as $\propto t^\delta$ with $\delta = (3/2)(\alpha + 1)$ and α an appropriate photon index (Wijers et al. 1997). If we use our best value of α_Γ for the decay part of the second pulse (-1.94 ± 0.13), we obtain $\delta = (-1.4 \pm 0.2)$, a value that is consistent with the observed decay of the GRB 970228 afterglow (Costa et al. 1997b). However, if we use the value of α_Γ determined at the end of the first pulse (-2.3 ± 0.3), the resulting value of δ (-1.95 ± 0.45) would not agree with our observations. The discontinuity in the γ-ray spectral index observed from the end of the first pulse to the beginning of the second pulse requires an interpretation. Given the continuity of the spectral index, starting from the second pulse, any physical relation between the X-ray component of the GRB and the afterglow emission most likely holds with the last set of hard GRB pulses, not with the first one. This suggests that the emission mechanism producing the X-ray afterglow might be already taking place after the first pulse.

This research is supported by the Italian Space Agency (ASI). K. H. is grateful to the US 1SAX Guest Investigator program for support.

REFERENCES

Amati, L., et al. 1997, Proc. SPIE, 3114, 176
Band, D., et al. 1993, ApJ, 413, 281
Boella, G., et al. 1997, A&AS, 122, 299
Costa, E., et al. 1997a, IAU Circ. 6572
———. 1997b, Nature, 387, 783
Feroci, M., et al. 1997, Proc. SPIE, 3114, 186
Ford, L. A., et al. 1995, ApJ, 439, 307
Frontera, F., Costa, E., Dal Fiume, D., Feroci, M., Nicastro, L., Orlandini, M., Palazzi, E., & Zavattini, G. 1997a, A&AS, 122, 357
Frontera, F., et al. 1997b, IAU Circ. 6637
———. 1997c, A&A, submitted
Guarnieri, A., et al. 1997, A&A, 328, 2
Hurley, K., et al. 1997, ApJ, 485, L1
Jager, R., et al. 1997, A&AS, 125, 557
Liang, E., Kusunose, M., Smith, I. A., & Crider, A. 1997, ApJ, 479, L35
Mészáros, P., & Rees, M. J. 1997, ApJ, 476, 232
Morrison R., & McCammon, D. 1983, ApJ, 270, 119
Murakami, T., Inoue, H., Nishimura, J., van Paradijs, J., Fenimore, E. E., Ulmer, A., & Yoshida, A. 1991, Nature, 350, 592
Sahu, K. C., et al. 1997, Nature, 387, 476
Tavani, M. 1996, ApJ, 466, 768
———. 1997, ApJ, 483, L87
van Paradijs, J., et al. 1997, Nature, 386, 686
Yoshida, A., et al. 1989, PASJ, 41, 509
Wijers, R. A. M. J., Rees, M. J., & Mészáros, P. 1997, MNRAS, 288, L51